



Microstructure, mechanical and thermal properties of YSZ thermal barrier coatings deposited by axial suspension plasma spraying

Olena Poliarus¹ · Jerzy Morgiel² · Wojciech Żórawski³ · Anna Góral² · Małgorzata Pomorska² · Krzysztof T. Wojciechowski⁴ · Oleksandr Cherniushok⁴

Received: 29 September 2022 / Revised: 11 January 2023 / Accepted: 26 January 2023 / Published online: 2 March 2023
© The Author(s) 2023, corrected publication 2023

Abstract

Yttrium-stabilized zirconia (YSZ) thermal barrier coatings (TBCs) are indispensable elements of present-day turbine propulsion systems. The ones deposited with atmospheric plasma spraying (APS) are characterized by required low thermal conductivity, but they are unable to survive frequent thermomechanical loading and therefore their application is limited to parts remaining stationary. Expanding capability of TBCs is sought in various areas, but the one realized through modification of most proliferated apparatus used for plasma spraying (PS) (from radial to axial injection) and substituting micrometric powders with the nano-structured suspension needs least changes in the industry established procedures and offers the highest property improvement. The present experiment covered the deposition of $ZrO_2-8Y_2O_3$ YSZ TBC using both atmospheric and suspension PS processes. They were performed with commercial micrometric and nano-structured YSZ (8% Y_2O_3) powders. The coatings morphology and microstructure were characterized with 3D profilometry, scanning and transmission electron microscopy (SEM/TEM) methods. Finally, the coating's hardness and heat conductivity were measured. This complex approach allowed to state that PS of micrometric t' - ZrO_2 powder having an admixture of m - ZrO_2 phase is capable of only partial improvement in its homogenization. However, the suspension PS process of nano-structured powder eliminated any traces of the monoclinic phase from the coating. The TEM microstructure observations indicated that the suspension PS coating is built by in-flight solidified droplets as well as by the melted ones flattened on arrival. A surface layer of liquefied material on solid droplets increases their adhesion to surface asperities promoting pseudo-columnar growth of the coating. The preservation of monotonic slow increase of thermal conductivity during heating of the suspension PS coating means, that its pseudo-columnar microstructure is better suited to withstand high strains during such treatment.

Keywords Yttrium-stabilized zirconia (YSZ) · Suspension plasma spraying (SPS) · Atmospheric plasma spraying (APS) · Thermal barrier coatings (TBC)

✉ Olena Poliarus
poliarus.o@imim.pl

¹ Frantsevich Institute for Problems of Materials Science, National Academy of Sciences of Ukraine (NASU), Krzhizhanovsky str, Kyiv 03142, Ukraine

² Institute of Metallurgy and Materials Science, Polish Academy of Sciences (PAS), 25 Reymonta St, 30-059 Krakow, Poland

³ Laser Processing Research Centre, Kielce University of Technology, 7 Tysiąclecia Państwa Polskiego Av, 25-314 Kielce, Poland

⁴ Department of Inorganic Chemistry, Faculty of Materials Science and Ceramics, AGH University of Science and Technology, Mickiewicza Ave. 30, 30-059 Krakow, Poland

1 Introduction

Thermal barrier coatings (TBCs) were introduced into the advanced aviation propulsion systems in the mid -1970s [1, 2]. Since then they have been used to insulate turbine metallic parts from hot combustion gases. In effect, it allowed to increase turbine operating temperature improving its efficiency at still acceptable durability. The main advantage of zirconia is related to its excellent mechanical properties represented by high fracture toughness and strength [3]. The ZrO_2 bested other ceramic materials as a TBCs candidate due to its very low thermal conductivity [4]. However, during cycling within the planned operating temperature range it undergoes a phase transformation from monoclinic (m - ZrO_2) to tetragonal (t - ZrO_2) phase (i.e., at 1170 °C), which

entails a significant volume change of ~ 4 vol. % [5]. The latter, in the case of ceramic material lacking potential for even small plastic deformation, means fast crack nucleation being the only way to release the transformation strains followed by coatings crumpling and delamination. The above issue was fixed by the addition of 6 to 9 vol. % of Y_2O_3 , which helps to stabilize the zirconia tetragonal phase (t' - ZrO_2), known also as yttria-stabilized zirconia (YSZ).

Choosing the deposition method of TBCs one should take into account that such protection can be guaranteed only by relatively thick coatings. Additionally, it should be possible to cover large areas of complicated shapes. The Electron Beam Physical Vapor Deposition (EB-PVD) and Atmospheric Plasma Spraying (APS) were able to satisfy both these requirements even in their original configuration [5, 6]. However, coatings produced with these methods differ strongly as it concerns morphology and microstructure, having direct implications as it concerns their resistance to the heat flow and the necessity to withstand mechanical strains developing between them and the metallic substrates. The APS coatings are built of on-impact flattened and then solidified droplets with extended porosity in-between [7, 8]. This process is securing their very low heat conductivity and high hardness but at a cost of only medium strain tolerance. The EB-PVD coatings are formed by columnar dendrite-like crystallites separated by numerous inter-column spacings open to penetration by hot gases [5]. It negatively affects their resistance to heat conductivity but helps to withstand frequent strain changes caused by temperature cycling. These differences in the properties of both types of coatings caused that the APS ones are a material of choice as it concerns the protection of more massive parts like a combustion chamber, while EB-PVD is predominantly applied on the turbine blades.

Producing YSZ coatings over large parts, like that for turbines, with the APS is much cheaper than with the EB-PVD method. Its application involves taking decisions on a number of parameters, which were probed with the aim to further optimize the TB properties. At first, the most promising action seemed to be straight swapping the coarse- with nano-powders [9, 10], what helped to homogenize and refine the coatings microstructure opening also a way for experiments with other admixtures into the zirconia [11, 12]. However, a high cost of such powders and their subsequent agglomeration required for proper work of the TS gun as well as up to $\sim 40\%$ material losses during this process canceled all the expected economic advantages. The more recent attempt also relies on the use of the nano-powders, but in the form of suspension. It was enabled by extended APS stand modification (known as Suspension Plasma Spraying/SPS) involving among the others re-directing of the powder supply lines from the PS gun nozzle (so-called Radial geometry) to the gun core (axial geometry) [13, 14]. It soon turned out, that

this new approach not only allowed to significantly, i.e., more than by half, cut on the nano-powder losses and on deposition time. Additionally, it allowed for a favorable modification of the coatings microstructure like the highly porous EB-PVD and securing low thermal conductivity rendering them proper for TRB applications [15]. The up till now published data on SPS experiments relate an effect of the feedstock, liquid carrier (alcohol, water-based, others) as well as deposition parameters on the coatings properties, morphology and meso-structure [13, 16]. The latter were investigated mostly with a scanning electron microscopy (SEM) method covering usually an arrangement of cracks and porosity, while more detailed microstructure investigations using transmission electron microscopy (TEM), proper for coatings produced with nano-powders are still lacking.

Therefore, the present work was aimed at comparing phase composition, morphology, roughness, hardness and heat conductivity of the YSZ (8% Y_2O_3) coatings deposited using SPS method with the industrially established APS one. A special emphasis was placed on microstructure characterization of deposited coatings using the TEM/STEM method.

2 Experimental techniques

The 8YSZ coatings (ZrO_2 —8 wt.% Y_2O_3) were deposited using plasma spray systems at Kielce University of Technology. It was done with a feedstock powder Metco 204 NS (Oerlikon Metco Europe GmbH) of $125 \mu m \pm 11 \mu m$ in size as well as water-based suspension of 8YSZ powder (particle size $< 2 \mu m$) from Northwest Mettech Corporation of Canada. The particles size distribution of commercial Metco 204 NS (Oerlikon Metco Europe GmbH) and 8YSZ powder (Northwest Mettech Corporation of Canada) were measured using HELOS particle Size Analysis (Sympatec GmbH, Germany).

The APS was performed using Plancer PN 120 stand with Thermal Miller 1264 feeder by applying power of $60 V \times 550 A$, powder feed rate 40 g/min and at a spraying distance of 100 mm. The SPS was done with the Northwest Mettech Corporation Canada Axial III stand equipped with Nano-Feed 350 system working at gas mixture composition 65% Ar, 15% N_2 , 20% H_2 , current 550 A, feed rate of 100 mL/min and a spraying distance of 50 mm. The coatings were deposited on sandblasted stainless steel plates (increasing its roughness up to $S_a \sim 5 \mu m$) with dimensions of $60 mm \times 26 mm \times 6 mm$. The roughness was measured with Talysurf CCI-Lite non-contact 3D profiler. The geometric parameters were measured according to ISO 25178 [17], and maps ($0.9 mm \times 0.9 mm$) illustrating the topography of deposits were presented. The coatings porosity was assessed using the Image J software.

The coatings morphology and cross-section microstructures were documented using scanning electron microscopy (SEM/E-SEM FEI XL 30), while phase composition with X-ray diffraction methods (XRD/D2 Phaser Bruker with $\text{CuK}\alpha$ radiation). The phase content of the powders and as-sprayed coatings were examined using the Diffrac EVA and HighScore Plus software with the ICDD PDF-4 + crystallographic database. Bragg-Brentano (Θ - 2Θ) X-ray diffraction continuous scans were performed over the range of $2\Theta = 10 \div 90^\circ$, with 0.02° step size and 2 s per step. The transmission electron microscope (TEM) by FEI (Tecnai F20 (200 kV)) with scanning transmission (STEM) unit, high angle annular dark field (HAADF) detector by Fishione and an integrated EDAX X-ray energy-dispersive spectroscopy (EDS) system was used to show deposit features in micro/nanoscale. Thin foils were cut out from the central part of the polished section of the coatings using FEI Quanta 200 Dual Beam FIB equipped with Omniprobe™ lift-out system.

Thermal diffusivity α_D was measured by the Netzsch LFA 457 equipment. The samples were firstly spray-coated with a thin layer of graphite to minimize errors from the emissivity of the material and laser beam reflection caused by a shiny pellet surface. For the calculation of thermal conductivity was used two-layer model as implemented in Proteus LFA Analysis and theoretically described by Hartmann et al. [18]. Prior to the measurements of YSZ-coated samples, the thermal diffusivity of the pure substrate was measured and then used in the two-layer model for the estimation of the thermal conductivity of YSZ coatings. Thermal conductivity of YSZ coatings was calculated using the equation $\kappa = dC_p\alpha_D$, where d and C_p are the density and the specific heat capacity taken from [19].

3 Results

Commercial YSZ Metco 204 NS powders were characterized by spherical shape and large scatter of size of diameter from a few micrometers up to $70 \mu\text{m}$ (Fig. 1a). On the other hand, powders fed from the suspension consisted of highly irregular particles of much smaller size $2 < \mu\text{m}$ (Fig. 1b).

Results of particles size distribution for both feedstocks are shown in Fig. 2.

For each of feedstock, measurements were made three times. The average particle size was: $d_{10} = 369 \mu\text{m}$; $d_{50} = 5191 \mu\text{m}$; $d_{90} = 7733 \mu\text{m}$ for powders and $d_{10} = 0,62 \mu\text{m}$; $d_{50} = 2463 \mu\text{m}$; $d_{90} = 7684 \mu\text{m}$ for suspension.

The SEM plan-view images indicated that the surface of APS-deposited coating was strongly corrugated and carried numerous bigger and smaller particles (Fig. 3a). In contrast, the surface of the SPS one was dominated by the presence of relatively large cauliflower-like top surface (Fig. 3b). The 2 D maps presenting distribution of local upheavals and recesses suggested that both coatings are characterized by similar roughness (Fig. 3c and d), as was confirmed by calculated roughness parameters given in Table 1.

The SEM images of sections of both produced coatings confirmed that the surface undulations were of comparable height (Fig. 4). Additionally they showed that the APS coating is characterized by wavy layered microstructure with frequent small and large porosity located at layer boundaries. The SPS-deposited coating turned out to be built of thick columnar grains filled with numerous fine porosity with larger pores located at column boundaries.

The STEM/ HAADF images of APS coating confirmed the presence of relatively thick curved and misshapen lamellas (Fig. 5a). Additionally they showed that even as

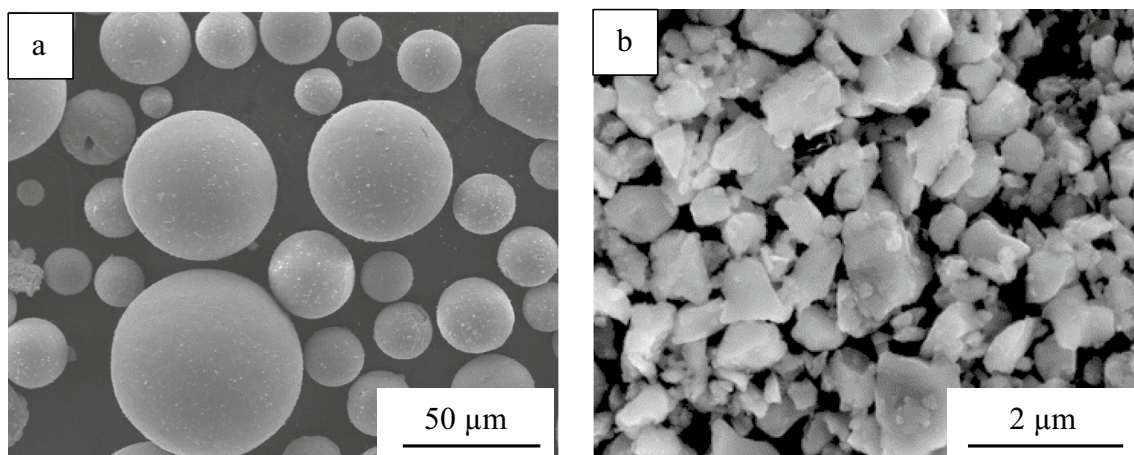


Fig. 1 SEM images of powders used in: a atmospheric and b suspension PS processes

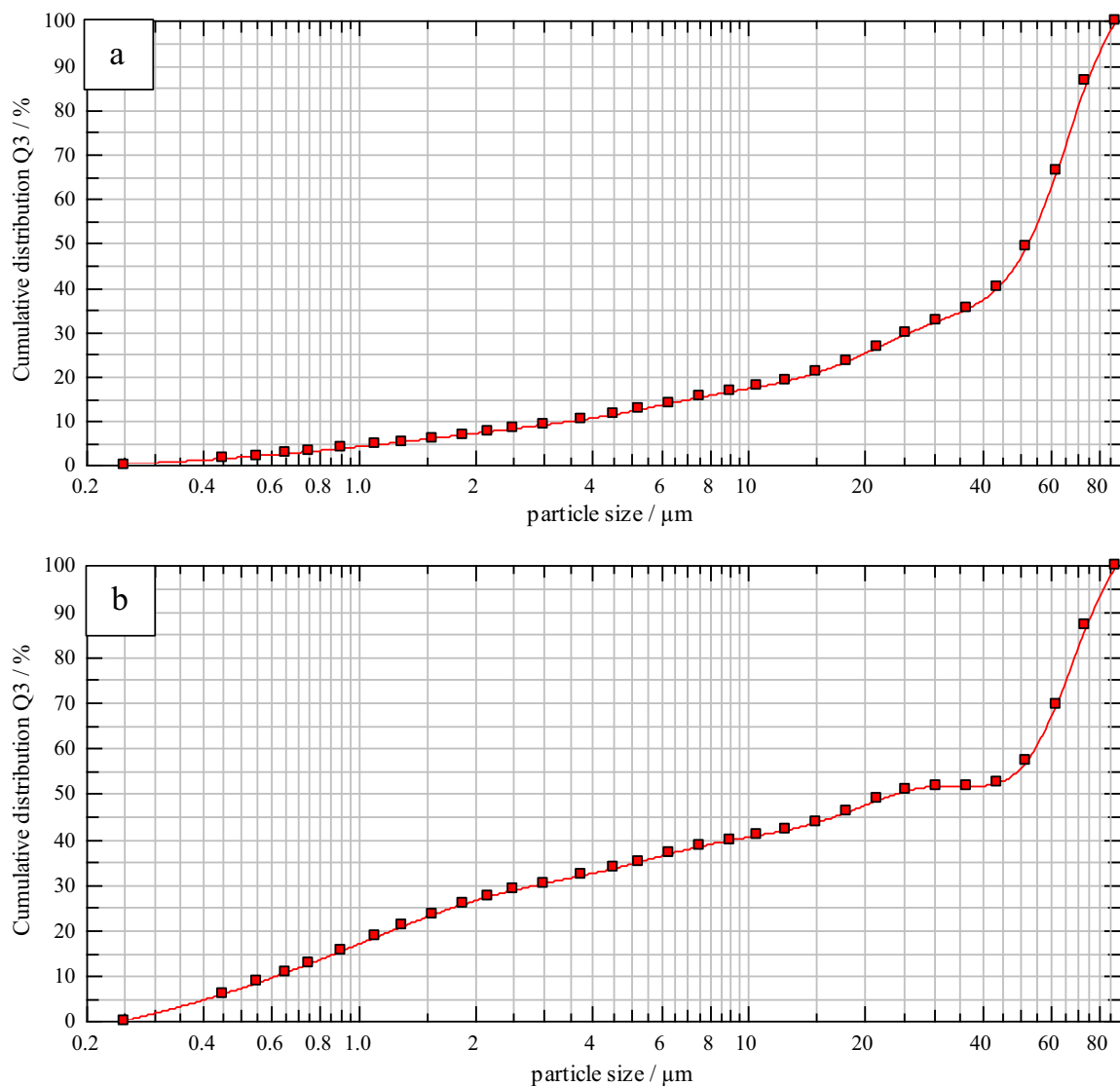


Fig. 2 The particles size distribution of: **a** commercial Metco 204 NS powder and **b** 8YSZ suspension (Northwest Mettech Corporation of Canada)

inter-layer porosity and cracks are dominating defects, though numerous through-layer cracks are also present (Fig. 5a). The latter usually propagate along boundaries of fine columnar crystallites filling in practically every layer. The observation with the same method of the SPS coating helped to establish that it is built mostly of rounded if not spherical sub-micrometer particles (Fig. 5b). It contains both small and large porosity, but they were usually separated with the exception of those located at the boundaries of thick columnar crystallites. The porosity of the deposited coatings increased from $\sim 10\%$ to 17.5% for APS and SPS method, respectively. Simultaneously, the size of the pores being within the $2\ \mu\text{m}$ to $5\ \mu\text{m}$ range for the former diminished down to $0.4\text{--}4\ \mu\text{m}$ for the latter (in the latter case the column diameter was of $\sim 20\ \mu\text{m}$).

The local chemical composition measurements performed using the EDS technique and presented as 2D mappings helped to establish that within the coating deposited using powder some of the layers indeed show a deficiency in yttrium content, as compared with neighboring ones (Fig. 5a). The map presenting distribution of Y is relatively noisy due to both its low amount in YSZ as well as the much lower intensity of the *K* than the *L* line, but at least *K* lines of Y and Zr are well spaced (see inset in the STEM-HAADF image) and therefore the obtained information is straightforward. The same measurements performed for the coatings obtained with the suspension showed none of the previously noted differences pointing to a more homogenous distribution of yttrium in the *t'*-ZrO₂ crystal lattice (Fig. 5b).

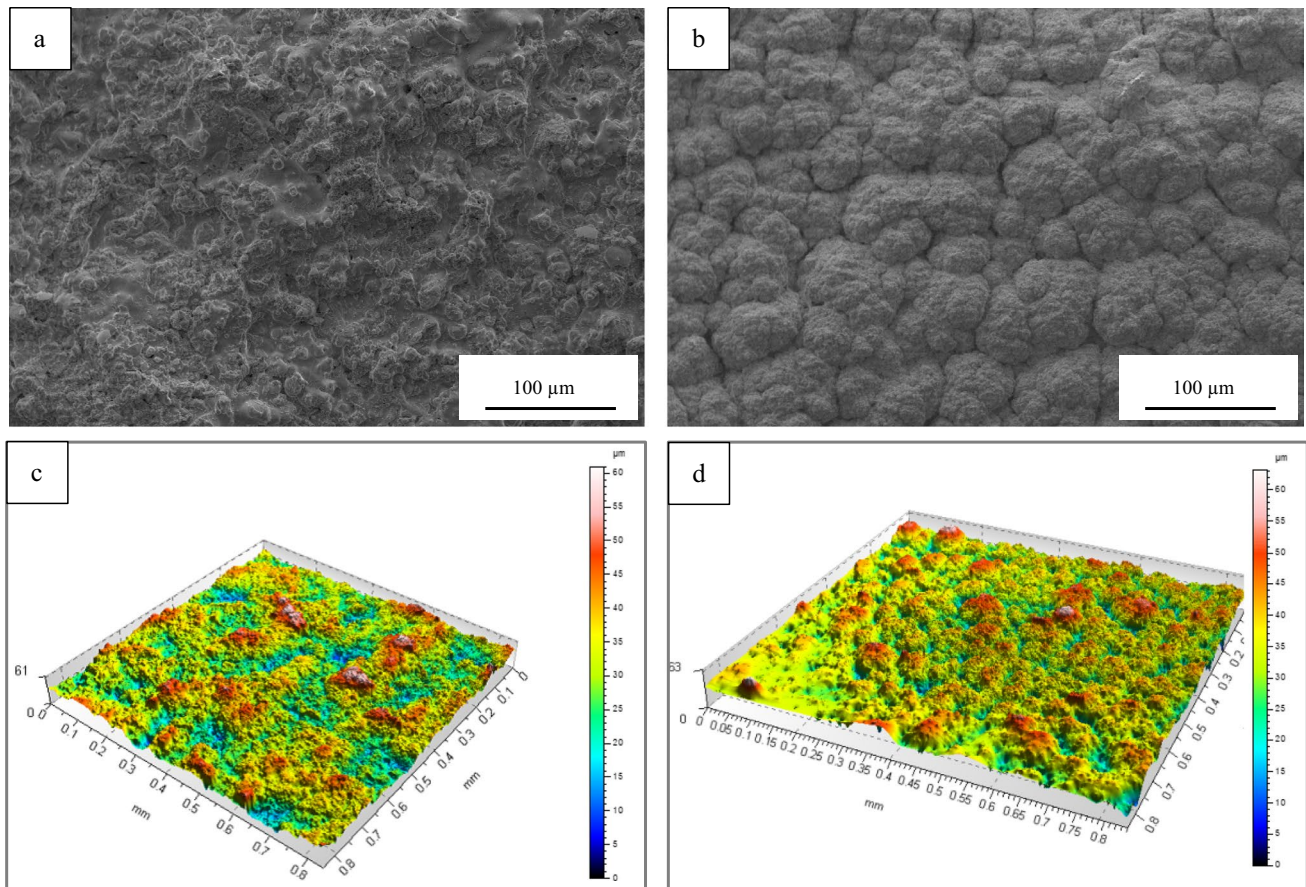


Fig. 3 SEM images of surface morphology of YSZ coatings deposited with: **a** atmospheric and **b** suspension PS processes accompanied by maps presenting their roughness (**c** and **d**, respectively)

Table 1 Parametrization of surface topography of APS- and SPS-deposited coatings

Parameter	ZrO ₂ -8Y ₂ O ₃ coating [μm]	
	SPS	APS
S _a	5.28	6.07
S _q	6.92	7.64
S _{sk}	-0.28	0.11
S _{ku}	3.89	3.11
S _p	28.95	28.95
S _v	34.35	32.05
S _z	63.30	61.01

S_a arithmetic mean height, S_q root mean squared height, S_{sk} skewness, S_{ku} kurtosis, S_p maximum peak height, S_v maximum valley depth, S_z maximum height

The TEM/ BF observations of the microstructure of the APS coating indicated that fine columnar crystallites in the layers frequently inherit orientations from that located below

them (Fig. 6a). Some of the columnar crystallites are filled with sets of needle-like plates, being a characteristic feature of the monoclinic zirconia (*m*-ZrO₂) phase (Fig. 6c). The SPS coatings turned-out to be built with fine and very fine mostly spherical or just rounded crystallites (Figs. 6b, 7a), while flattened ones were noted only occasionally (Fig. 7b). The higher magnifications pointed the former crystallites were fused with the other ones only locally forming small necking's and contributing to the formation of closed small porosity in their vicinity. The latter crystallites tend to half-envelop their neighbors promoting the development of a much denser microstructure (Fig. 7b). Interestingly, while the rounded or spherical crystallites were in each case of the same orientation, though the flattened ones were filled with sets of very fine columnar crystallites. The high magnification observations indicated that two type of processes take part during coating deposition, i.e., attachment of in-flight fully solidified particles with the help of solid-state diffusion taking place at the surface of only partly cooled particles as documented in Fig. 8a, well as their binding with the surrounding material by particles arrived in the liquid state as shown in Fig. 8b.

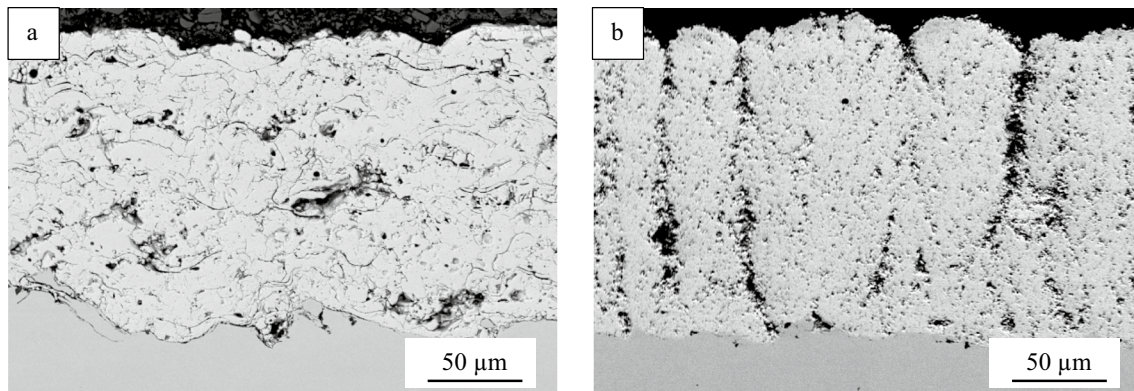


Fig. 4 SEM images of YSZ coatings deposited with: **a** atmospheric and **b** suspension PS processes

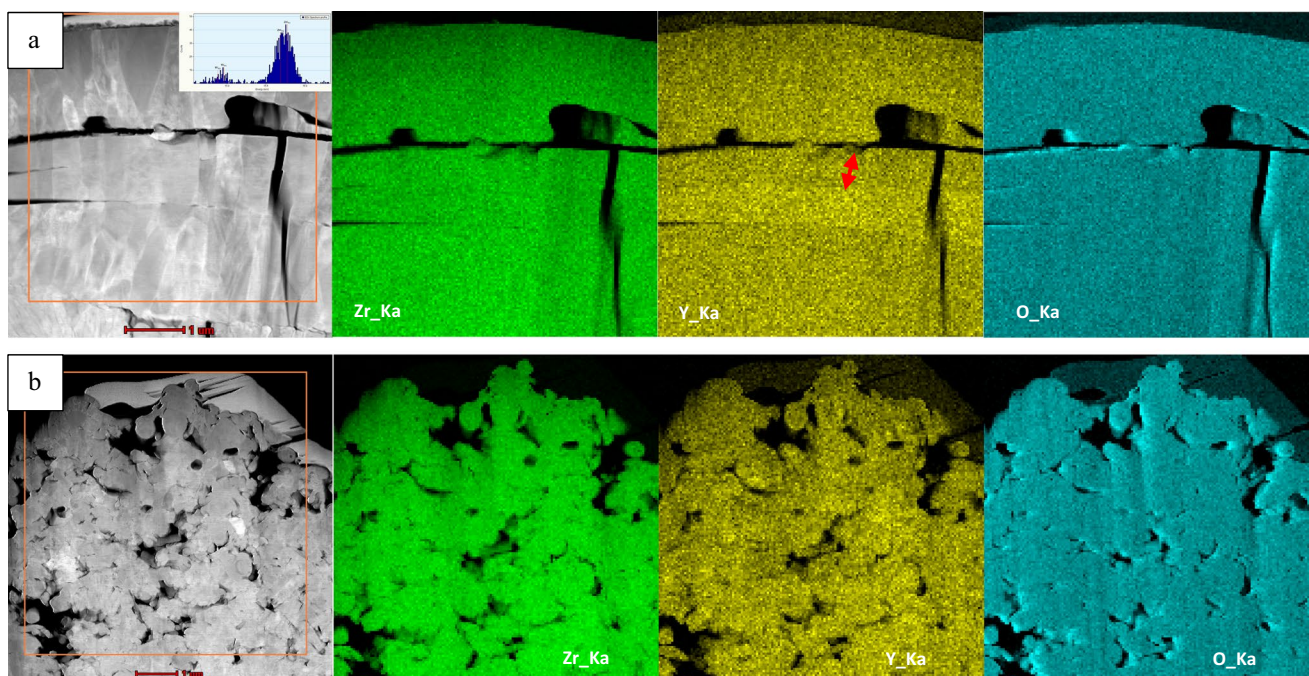


Fig. 5 STEM/ HAADF images of YSZ coatings deposited with: **a** atmospheric and **b** suspension PS processes and maps presenting distribution of Zr, Y and O (double arrow shows layer depleted in Y)

The phase composition assessed with the XRD method of as-supplied YSZ powder used for APS deposition showed that it contains not only the tetragonal (t' -ZrO₂, 85.3(1) wt.%) phase with cell parameters $a = 3.615(1) \text{ \AA}$, $c = 5.163(1) \text{ \AA}$ but also a low fraction (14.7(2) wt.%) of monoclinic one (m -ZrO₂) with parameters: $a = 5.155(1) \text{ \AA}$, $b = 5.207(1) \text{ \AA}$, $5.317(1) \text{ \AA}$, $\alpha = 90^\circ$, $\beta = 99.2(1)^\circ$, $\gamma = 90^\circ$ (Fig. 9a). The X-ray diffraction spectra obtained from the coating produced from this powder also bear traces of monoclinic phase ($a = 5.164(3) \text{ \AA}$, $b = 5.203(3) \text{ \AA}$, $c = 5.308(3) \text{ \AA}$, $\alpha = 90^\circ$, $\beta = 99.2(9)^\circ$, $\gamma = 90^\circ$), although much smaller (3.6(2) wt.%) than that measured in the

powder. Weight fraction of t' -ZrO₂ phase within it was 96.4(1) wt.%, while cell parameters of this phase equaled to: $a = 3.613(1) \text{ \AA}$, $c = 5.162(1) \text{ \AA}$.

The XRD measurements of dried suspension intended for SPS deposition also showed the peaks corresponding to both tetragonal (t' -ZrO₂, 75(7) wt.%, $a = 3.61(3) \text{ \AA}$, $c = 5.2(5) \text{ \AA}$) and monoclinic m -ZrO₂ type phases (25(2) wt.%, $a = 5.2(3) \text{ \AA}$, $b = 5.2(2) \text{ \AA}$, $c = 5.2(4) \text{ \AA}$, $\alpha = 90^\circ$, $\beta = 98(1)^\circ$, $\gamma = 90^\circ$) (Fig. 9b). The set of peaks recorded from the coatings produced from the suspension sharpened and belonged only to tetragonal type phase ($a = 3.616(1) \text{ \AA}$, $c = 5.159(1) \text{ \AA}$).

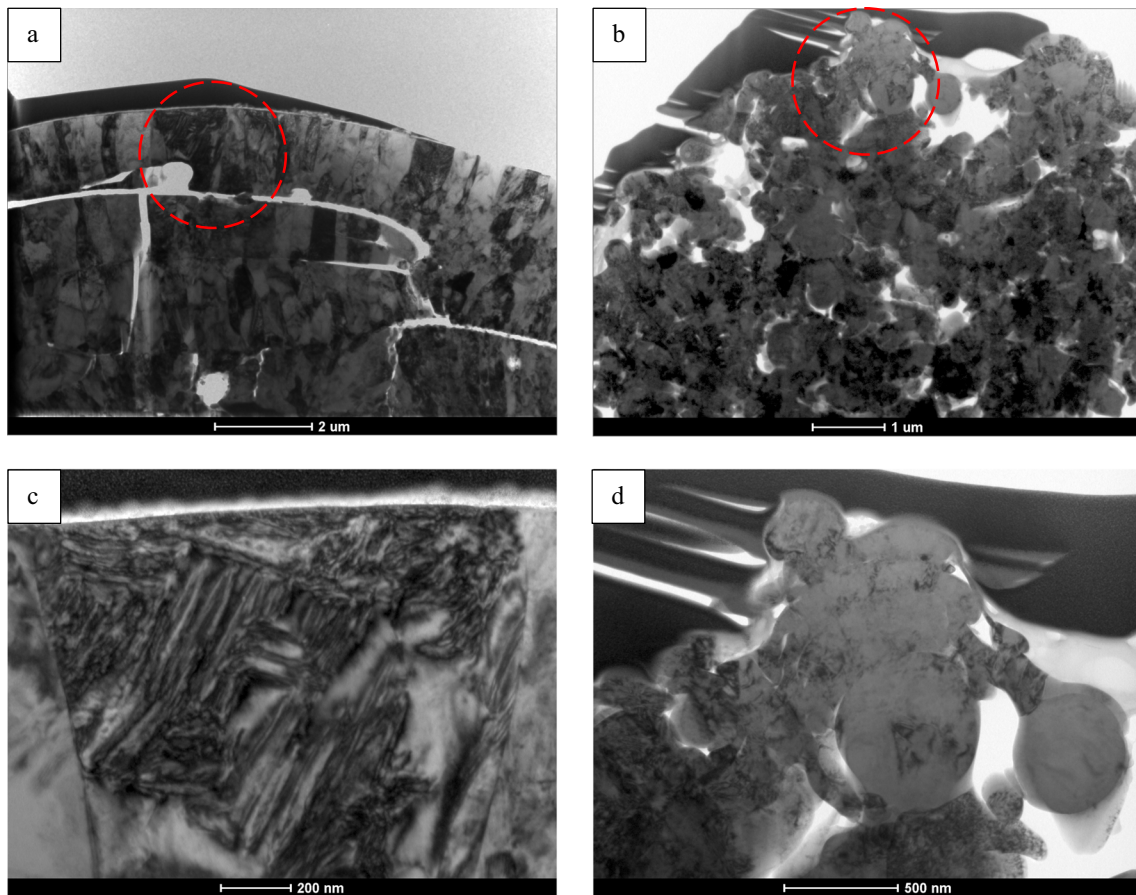


Fig. 6 TEM/BF images of YSZ coatings deposited with: **a, c** atmospheric and **b, d** suspension PS processes (lower ones present details taken in circle in upper respective images)

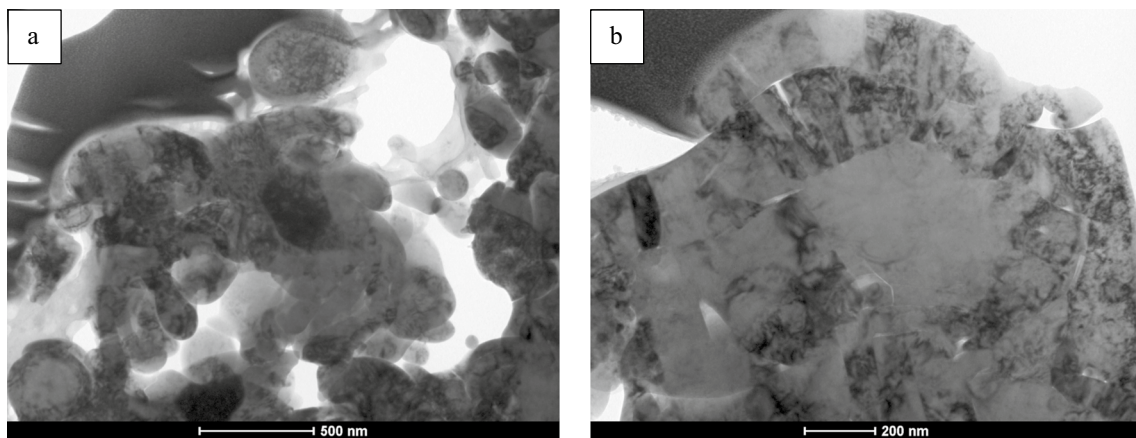


Fig. 7 TEM/BF images presenting two types of characteristic microstructure of YSZ coating-deposited suspension PS: **a** colonies of rounded crystallites and **b** mixed rounded and flattened ones

The micro-hardness test showed a significant scatter of results but an average of several measurements under a larger load were both close to ~ 400 HV0.1 with a relatively small

scatter $< 10\%$ (Table 2). Diminishing the load (HV0.05) produced lower micro-hardness values for coating obtained using solution while the one deposited using the atmospheric

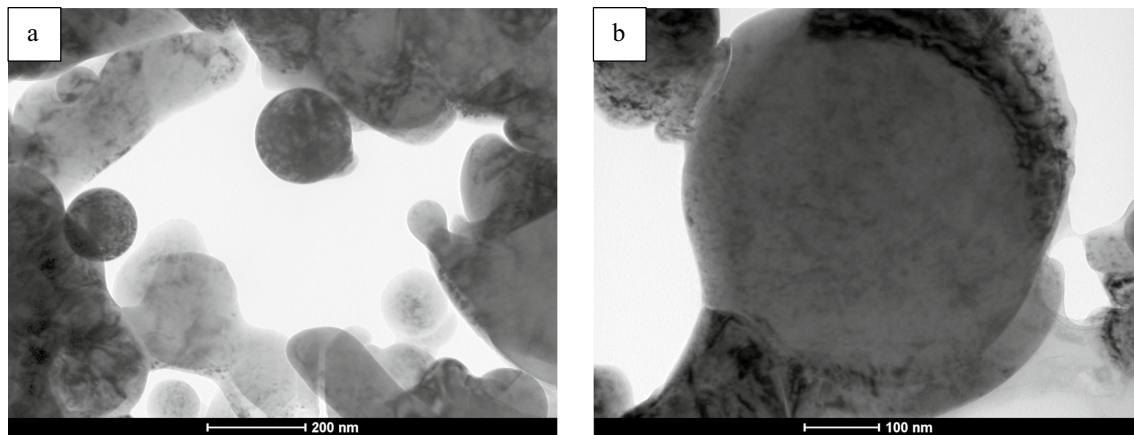


Fig. 8 TEM/BF images presenting in-flight solidified spherical particles of YSZ imbedded into suspension PS coating attached with the help of: **a** solid state diffusion and **b** wetting of liquids

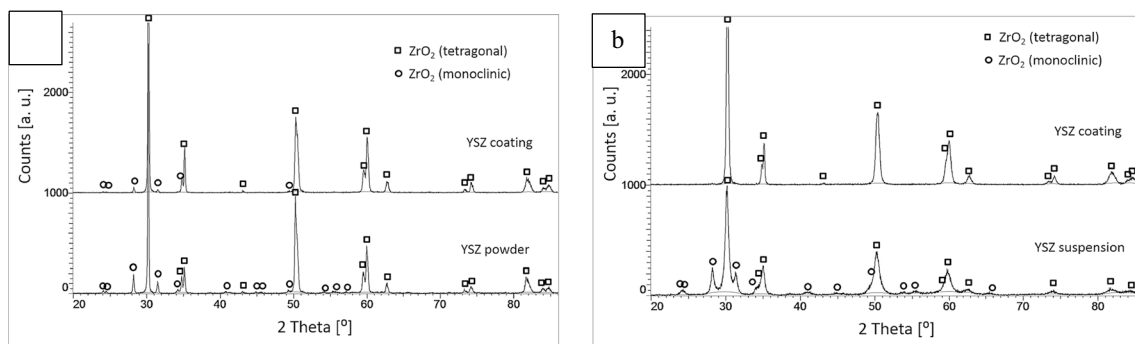


Fig. 9 XRD spectra of powders and coatings from: **a** atmospheric and **b** suspension PS processes

Table 2 Hardness measurements at polished sections of APS- and SPS-deposited coatings

Place of measurement	ZrO ₂ -8Y ₂ O ₃			
	SPS coating		APS coating	
	HV0.05	HV0.1	HV0.05	HV0.1
Coating center	366 ± 6	419 ± 6	404 ± 9	414 ± 5
“Porosity-less” areas	–	460 ± 2	–	500 ± 2

PS process remain practically the same even as the scatter in measured values was nearly doubled as compared with the HV0.1 test.

The thermal conductivity at RT of the suspension PS-deposited coatings were more than times higher than the one deposited from the powder, i.e., $1.6 \text{ Wm}^{-1} \text{ K}^{-1}$ and $0.7 \text{ Wm}^{-1} \text{ K}^{-1}$, respectively (Fig. 10a). In both cases, it was rising same up to $400 \text{ }^\circ\text{C}$ at a rate of $\sim 0.003 \text{ Wm}^{-1} \text{ K}^{-2}$, while above that temperature the thermal conductivity stabilized for the one deposited using suspension and lowered in case of the one deposited with the powder. The thermal resistivity

at RT of the steel substrate protected with respective coating turned out practically the same being close to $2 \text{ cm}^2\text{KW}^{-1}$ (Fig. 10b). With a rise of temperature, it was decreasing slightly faster in the case of substrate plus suspension coatings falling at $800 \text{ }^\circ\text{C}$ to $1 \text{ cm}^2\text{KW}^{-1}$, while for the other one it was still at the level of $1.5 \text{ cm}^2\text{KW}^{-1}$.

4 Discussion

The complex morphology of atmospheric PS coatings, characterized by numerous cavities and hillocks, is a direct result of their deposition over sandblasted and therefore highly roughened surfaces. The incoming melted powder particles flatten on impact delineating all the unevenness located below and producing layered-wavy microstructure with frequent porosity in-between them (Fig. 4a). The above mechanism was noted previously for most other ceramic PS coatings [7, 10, 12]. The morphology of the coatings deposited using the suspension PS technique is dominated by the presence of finely textured cupolas crowning columnar grains

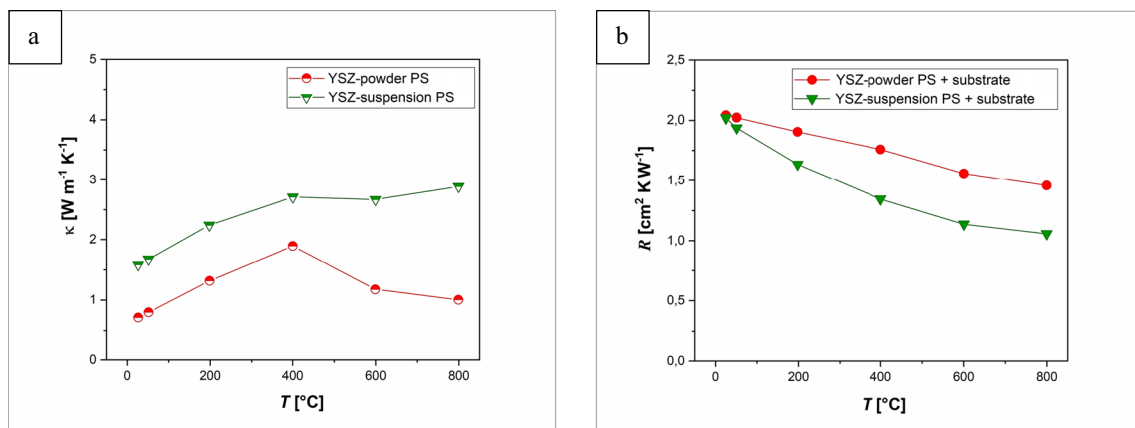


Fig. 10 Thermal conductivity of YSZ coatings deposited with atmospheric and suspension PS processes (a) and corresponding thermal resistivity of coating and substrate (b)

separated by deep grooving over pseudo-columnar grain boundaries as shown in (Fig. 4b). The coatings produced with the latter process are also deposited over sandblasted substrates, but in this case, the coatings surface morphology frequently bears no evidence of the previous treatment. Therefore, even as the measurements of the surface roughness locate the atmospheric and suspension PS coatings very close to each other (Table 1), though such a situation is just a coincidence, as their morphology is developed by the action of altogether different processes.

The pseudo-columnar growth of the nano-structured suspension PS YSZ coatings has turned out to be sensitive to a number of deposition parameters like the average particle size, liquid carrier composition, flow rate, the ratio of solid to liquid, and stand-off distance [13, 16, 20–22]. The formation of this characteristic microstructure is sought in the operation of strong drag force exerted on in-flight solidified drops by a working gas, which is surpassing the adhesion force on the impact on a flat surface [23, 24]. The present TEM observations showed that the microstructure of the suspension PS coatings is built both of in-flight solidified or at least partly solidified fine drops of melted YSZ powder particles as well as of the liquid ones. Additionally, nearly all in-flight solidified particles easily recognized by their close to perfect spherical shape were connected with the other particles in the coating by necking. It means that a significant fraction of powder is first melted into drops, solidifies, and is next wetted by unsolidified ones. In this way, the solid core builds up the drag force pushing the particle along the substrate, while the liquid layer at its surface is responsible for attaching it to any larger asperity. The fine surface texture over each of the domes is witnessing the fact that they are built of these very small droplets solidified on-flight.

The introduction of up to 8 wt. % of yttrium oxide into tetragonal (*t*-ZrO₂) zirconia should help to stabilize it into tetragonal (*t'*-ZrO₂) phase, but our XRD measurements showed that

both presently used commercial powders showed the presence of a significant portion of monoclinic (*m*-ZrO₂). The latter phase was also detected in the XRD spectra acquired from powder PS coating, but not with the one deposited using suspension. It was probably caused by local inhomogeneity of the commercial powders (such a situation had arisen also in other works [6, 8]), what in case of the coarser powder was transferred on the atmospheric PS coating (even as in a visibly diminished fraction), as documented on respective EDS maps of local chemical composition. The above result indicates that even as during the both processes practically all particles undergo melting, though in the micrometric powder used in atmospheric PS less of them are subjected to in-flight merging than in with the case of nano-structured powder used in suspension. Simultaneously, the presence of the small fraction of *m*-ZrO₂ in the atmospheric PS coating might have arisen of its much coarser microstructure and therefore the development of higher strains during cooling. The presently performed TEM observations showed that the strain accumulated in the layered structure is relieved either by the development of vertical cracks along the boundaries of fine columnar crystallites or by changing them to the monoclinic phase. Both of these possibilities operate independently, but their occurrence would be in each case highly damaging for the coating during its thermal cycling.

The crucial functional parameter for TBC, i.e., the thermal conductivity (TC) of the presently investigated coatings was more than two times higher in the case of the suspension PS than the one deposited from powder PS, which corresponds to the results obtained within other experiments with the material of similar composition [4, 24, 25]. With increasing temperature the TC of these two coatings was rising like in other experiments [24, 26], but above 400 °C in case of powder atmospheric PS coating, it started to lower unexpectedly. This collapse of the monotonic rise of TC can be connected only with some

catastrophic changes in the coating microstructure like development of local cracks at the coating /substrate interface and increasing volume of closed porosity in that area. The above events were reported also for suspension PS coatings [20], which were lacking a proper nickel-based super-alloy buffer layer decreasing the strain developing between the two. The suspension PS coatings deposited within this work also showed some lowering of TC in discussed temperature range, but on the much lower scale.

5 Summary

The described experiment covers a complex characterization of the morphology and microstructure as well as measurements of chosen properties including hardness and thermal conductivity of the PS coatings deposited using dry powder and suspension. It confirmed that in the case of powders of micrometric YSZ (t' -ZrO₂ having an admixture of m -ZrO₂) the atmospheric PS process causes only partial improvement in the homogenization of deposited material assessed by a decrease, but not the elimination of the monoclinic phase. On the other hand, the smaller size of the nanostructured powder and its longer passage within the plasma in the suspension PS process eliminated any traces of the monoclinic phase from the coating. The TEM microstructure observations proved that the coating is built both by in-flight solidified droplets and by the melted ones, which are flattened on arrival. Additionally, the former are frequently coated with the liquefied material increasing their adhesion to surface asperities promoting pseudo-columnar growth of the coating. The observation that a numerous in-flight solidified particles are attached with the surrounding material by relatively weak binding achieved with the solid-stated diffusion active during the cooling-off period means, that the careful optimization of deposition condition by adjusting first of all the gun/substrate distance it is possible to improve the connection between the particles and in the effect the mechanical properties of the coatings.

The formation of plate-like microstructure in the apex of bent parts of flattened-on-arrival drops during the atmospheric PS process indicates that the m -ZrO₂ may develop not only due to local depletion in yttrium but also due to high local strain level. The preservation of monotonic slow increase of thermal conductivity during heating of the suspension PS coating deposited directly on steel substrate means, that its pseudo-columnar microstructure is better suited to stand high strains developing during such treatment than the one PS deposited using the dry powder. It confirms that the voids at the column boundaries are indeed a favorable feature of the microstructure of the TBC.

Acknowledgements The work was done within the research stay of Olena Poliarus at Institute of Metallurgy and Materials Science supported by Polish Academy of Science

Author contributions All authors contributed to the study conception and design. Material preparation, data collection and analysis were performed by Dr. Anna Góral, Prof. Jerzy Morgiel, Prof. Krzysztof T. Wojciechowski, Prof. Wojciech Żórawski, Dr. Olena Poliarus, Mgr. Małgorzata Pomorska and Oleksandr Cherniushok. The first draft of the manuscript was written by Dr. Olena Poliarus and Prof. Jerzy Morgiel, and all authors commented on previous versions of the manuscript. All authors read and approved the final manuscript.

Data availability We confirm that all data can be available.

Declarations

Conflict of interest All authors declare that they have no conflicts of interest.

Ethical approval Not applicable.

Open Access This article is licensed under a Creative Commons Attribution 4.0 International License, which permits use, sharing, adaptation, distribution and reproduction in any medium or format, as long as you give appropriate credit to the original author(s) and the source, provide a link to the Creative Commons licence, and indicate if changes were made. The images or other third party material in this article are included in the article's Creative Commons licence, unless indicated otherwise in a credit line to the material. If material is not included in the article's Creative Commons licence and your intended use is not permitted by statutory regulation or exceeds the permitted use, you will need to obtain permission directly from the copyright holder. To view a copy of this licence, visit <http://creativecommons.org/licenses/by/4.0/>.

References

1. Miller RA. Thermal barrier coatings for aircraft engines: History and directions. *J Therm Spray Technol.* 1995;6:35–42. <https://doi.org/10.1007/BF02646310>.
2. Vaßen R, Jarligo MO, Steinke T, Mack D, Stover D. Overview on advanced thermal barrier coatings. *Surface Coatings Technol.* 2010;205:938–42. <https://doi.org/10.1016/j.surfcoat.2010.08.151>.
3. Pawłowski L, Blanchart Ph. Industrial chemistry of oxides for emerging applications. 2018; <https://doi.org/10.1002/9781119424079>
4. Clarke DR, Philipot SR. Thermal barrier coating materials. *Materials Today.* 2005;6:22–9.
5. Boissonnet G, Chalk C, Nicholls JR, Bonnet G, Pedraza F. Phase stability and thermal insulation of YSZ and erbia-yttria co-doped zirconia EB-PVD thermal barrier coating systems. *Surface Coat Technol Elsevier.* 2020;389:125566. <https://doi.org/10.1016/j.surfcoat.2020.125566>.
6. Vassen R. Thermal barrier coatings. Chapter II in *Ceramics Science and Technology.* Riedel R, I-Wei Chen (Eds). 2013; <https://doi.org/10.1002/9783527631971.cho2>.
7. Lima RS. Porous APS YSZ TBC manufactured at high powder feed rate (100 g/min) and deposition efficiency (70%): microstructure, bond strength and thermal gradients. *J Therm Spray Technol.* 2022;31:396–414. <https://doi.org/10.1007/s11666-021-01302-y>.
8. Patterson T, Leon A, Jayaraj B, Liu J. Thermal cyclic lifetime and oxidation behaviour of air plasma sprayed CoNiCrAlY bond coats

- for thermal barrier coatings. *Surf Coat Technol.* 2008;203:437–41. <https://doi.org/10.1016/j.surfcoat.2008.08.054>.
9. Fauchais P, Vardelle AM, Vardelle M. Thermally sprayed nanoceramic and nanocomposite coatings. 2015; <https://doi.org/10.1016/B978-0-12-799947-0.00010-9>
 10. Ghasemi R, Vakiliifard H. Plasma-sprayed nanostructured YSZ thermal barrier coatings: Thermal insulation capability and adhesion strength. *Ceram Int.* 2017;43:8556–63. <https://doi.org/10.1016/j.ceramint.2017.03.074>.
 11. Sanches E, Bannier E, Cantavella V, Salvador MD, Kleyatskina E, Morgiel J, Grzonka J, Boccacini AR. Deposition of Al₂O₃-TiO₂ nanostructured powders by atmospheric plasma spraying. *J Therm Spray Technol.* 2008;17:329–37. <https://doi.org/10.1007/s11666-008-9181-5>.
 12. Góral A, Żórawski W, Lityńska-Dobrzyńska L. Study of the microstructure of plasma sprayed coatings obtained from Al₂O₃-13TiO₂ nanostructured and conventional powders. *Mater Charact.* 2014;96:234–40. <https://doi.org/10.1016/j.matchar.2014.08.016>.
 13. Mauer G, Jarligo MO, Marcano D, Rezanka S, Zhou D, Vassen R. Recent developments in plasma spray processes for applications in energy technology, 19th Chemnitz Seminar on Materials Engineering – 19, IOP Conf. Ser.: Mater Sci Eng 2017;181: 012001 <https://doi.org/10.1088/1757-899X/181/1/012001>.
 14. Miranda F, Caliarì F, Essiçhtchouk A, Pertraconi G. Atmospheric plasma spray processes: from micro to nanostructures, in atmospheric pressure from diagnostic to applications, (Ed.) Nikiforov A, Chen Z <https://doi.org/10.5772/intechopen.80315>.
 15. Kozerski S, Łatka L, Pawłowski L, Cernuschi F, Petit F, Pierlot Ch, Podlesak H, Laval J-P. Preliminary study on suspension plasma sprayed ZrO₂ + 8 wt% Y₂O₃ coatings. *J Eur Ceram Soc.* 2011;31(12):2089–98. <https://doi.org/10.1016/j.jeurceramsoc.2011.05.014>.
 16. Yaghtin M, Yaghtin A, Najafisayar P, Tang Z, Troczynski T. Aging behavior of water-based YSZ suspensions for plasma spraying of thermal barrier coatings. *J Therm Spray Technol.* 2021;30:97–107. <https://doi.org/10.1007/s11666-021-01162-6>.
 17. ISO 25178–2:2012: Geometrical product specifications (GPS) - Surface texture: Areal - Part 2: Terms, definitions and surface texture parameters.
 18. Hartmann J, Nilsson O, Fricke J. Thermal diffusivity measurements on two-layered and three-layered systems with the laser-flash method. *High Temp High Press.* 1993;25:403–10.
 19. Radovic M, Lara-Curzio E, Trejo RM, Wang H, Porter WD. Thermophysical properties of YSZ and Ni-YSZ as a function of temperature and porosity. In advances in solid oxide fuel cells II: ceramic engineering and science proceedings (Eds) Bansal NP, Wereszczak A, Lara-Curzio E. 2006; <https://doi.org/10.1002/9780470291337.ch8>.
 20. Zhou D, Guillon O, Vaßen R. Development of YSZ thermal barrier coatings using axial suspension plasma spraying. *Coatings.* 2017;7:120. <https://doi.org/10.3390/coatings7080120>.
 21. Sokołowski P, Björklund S, Musalek R, Candidato RT Jr, Pawłowski L, Nait-Ali B, Smith D. Thermophysical properties of YSZ and YCeSZ suspension plasma sprayed coatings having different microstructures. *Surf Coat Technol.* 2017;318:28–38. <https://doi.org/10.1016/j.surfcoat.2017.02.054>.
 22. Tarasi F, Alebrahim E, Dolatabadi A, Moreau C. A comparative study of YSZ suspensions and coatings. *Coatings.* 2019;9:188. <https://doi.org/10.3390/coatings9030188>.
 23. Ekberg J. Investigation of microstructure and porosity of columnar yttria-stabilized zirconia coatings produced by axial suspension plasma spraying, Chalmers University of Technology, Technical report no 114/2017, ISSN 1652–8891.
 24. Van Every K, Krane MJM, Trice RW, Wang H, Porter W, Besser M, Sordelet D, Ilavsky J, Almer J. Column formation in suspension plasma-sprayed coatings and resultant thermal properties. *J Therm Spray Technol.* 2011;20:817–28. <https://doi.org/10.1007/s11666-011-9632-2>.
 25. Łatka L, Cattinia A, Pawłowski L, Valette S, Pateyron B, Lecompte J-P, Kumar R, Denoirjean A. Thermal diffusivity and conductivity of yttria stabilized zirconia coatings obtained by suspension plasma spraying. *Surf Coat Technol.* 2012;208:87–91. <https://doi.org/10.1016/j.surfcoat.2012.08.014>.
 26. Ganvir A, Curry N, Markocsan N, Nylén P, Toma F-L. Comparative study of suspension plasma sprayed and suspension high velocity oxy-fuel sprayed YSZ thermal barrier coatings. *Surf Coat Technol.* 2015;268:70–6. <https://doi.org/10.1016/j.surfcoat.2014.11.054>.

Publisher's Note Springer Nature remains neutral with regard to jurisdictional claims in published maps and institutional affiliations.